Realization of High-Stability Flat-Top Pulsed Magnetic Fields by a Bypass Circuit of IGBTs in the Active Region

Shaozhe Zhang, Zhenglei Wang, Tonghai Ding, Houxiu Xiao, Jianfeng Xie, and Xiaotao Han, *Member, IEEE*

***Abstract*—A high-stability flat-top pulsed magnetic field (FTPMF) is strongly needed for some scientific studies, such as nuclear magnetic resonance and specific heat measurement. This paper presents a new linear flat-top regulation bypass circuit to generate a high-stability FTPMF based on a battery bank power supply. The bypass circuit consists of insulated-gate bipolar transistors (IGBTs) in parallel that operate in the active region and are free of switch ripples. To achieve precise control of the IGBT current, the influence of the Miller effect and the nonlinearity of the IGBT's transfer characteristic are studied in detail. Then, a dual-feedback loop is designed and analyzed. A prototype consisting of a 1000 V/30 kA battery bank and a bypass circuit of 1700 V/3600 A IGBTs is developed. An FTPMF with a field/duration of 23.370 T/100 ms and a stability of 64.2 ppm has been achieved.**

***Index Terms*—Active region, bypass circuit, flat-top pulsed magnetic field (FTPMF), high stability, insulated-gate bipolar transistor (IGBT), switch ripple free.**

I. Introduction

THE high magnetic field is one of the most important tool in experimental physics for discovering unknown phenomena and providing higher resolution of a resonance [1]. In some scientific studies, such as nuclear magnetic resonance and specific heat measurement, a high stability (<100 ppm) of the magnetic field during the equilibration time (>10 ms) of a sample is necessary to gain a sufficiently good signal-to-noise ratio [2]. The flat-top pulsed magnetic field (FTPMF), which has both a high field strength and a high field stability, is the best choice for these scientific studies. In recent years, many methods have been proposed to improve the performance of the FTPMF [3]–[7]. However, generating an FTPMF with a long flat-top duration (>100 ms) and a high stability (<100 ppm) is still challenging.

There are mainly three types of power supplies that generate FTPMFs: the ac flywheel generator, the capacitor bank, and the lead-acid battery bank [8]. The output voltage of an ac flywheel generator is controllable; accordingly, it can generate diverse pulsed field shapes. FTPMFs with fields/durations of 60 T/100 ms, 45 T/850 ms, and 27 T/2.6 s are achieved based on a 1.43 GVA/650 MJ ac flywheel generator with a 12-pulse rectifier at the National High Magnetic Field Laboratory in the USA [3]. The Wuhan National High Magnetic Field Center (WHMFC) in China produces a 50 T/100 ms FTPMF in the same way [4]. However, the residual ripple of the 12-pulse rectifier is inevitable, which makes the stability of the FTPMF no better than 0.5% [5].

Although the capacitor bank has the advantages of high voltage and no ripple, it is hard to generate a flat-top profile with this method as its output voltage drops uncontrollably. A method coupling two discharge circuits by a pulsed transformer has been proposed based on a capacitor bank power supply, and the FTPMF can be obtained by a combination of the discharge trigger times [5]. An FTPMF of 41 T/6 ms/0.2% has been achieved with this technique at the WHMFC. Nevertheless, the requirements of the circuit parameters and trigger timing are very strict in this system, and it is difficult to improve the stability and duration. In [6], a minicoil powered by a battery bank is embedded into the main magnet driven by a capacitor bank to regulate the magnetic field profile. In this system, metal–oxide–semiconductor field-effect transistors (MOSFETs) as controllable resistors are in series with the minicoil to adjust the magnetic field so that the superimposed magnetic field can have a flat-top shape. An FTPMF of 60.64 T/2 ms/82 ppm is accomplished by this technique at the Institute for Solid State Physics in Japan. Similarly, an insulated-gate bipolar transistor (IGBT) as a controllable resistor is connected to the circuit in series to regulate the magnetic field [9]–[11]. However, limited by the maximum rated values of the IGBT, it is impractical to connect IGBTs to the magnet in series when the current is more than tens of kiloamperes. Although a relatively high magnetic field strength can be obtained based on the capacitor bank power supply, it is difficult to make the duration of the FTPMF longer than 10 ms as the output voltage drops rapidly.

Manuscript received June 1, 2019; accepted July 17, 2019. Date of publication July 28, 2019; date of current version December 13, 2019. This work was supported by the National Key Research and Development Plan Project of China (2016YFA0401703). Recommended for publication by Associate Editor H. H-C. Iu. *(Corresponding author: Xiaotao Han.)*

The authors are with Wuhan High Magnetic Field Center and the College of Electrical and Electronics Engineering, Huazhong University of Science and Technology, Wuhan 430074, China (e-mail: shaozhezhang@hust.edu.cn; zilaywang@hust.edu.cn; thding@mail.hust.edu.cn; xiaohouxiu@mail.hust.edu.cn; xiejianfeng@hust.edu.cn; xthan@hust.edu.cn).

Color versions of one or more of the figures in this paper are available online at http://ieeexplore.ieee.org.

Digital Object Identifier 10.1109/TPEL.2019.2931488

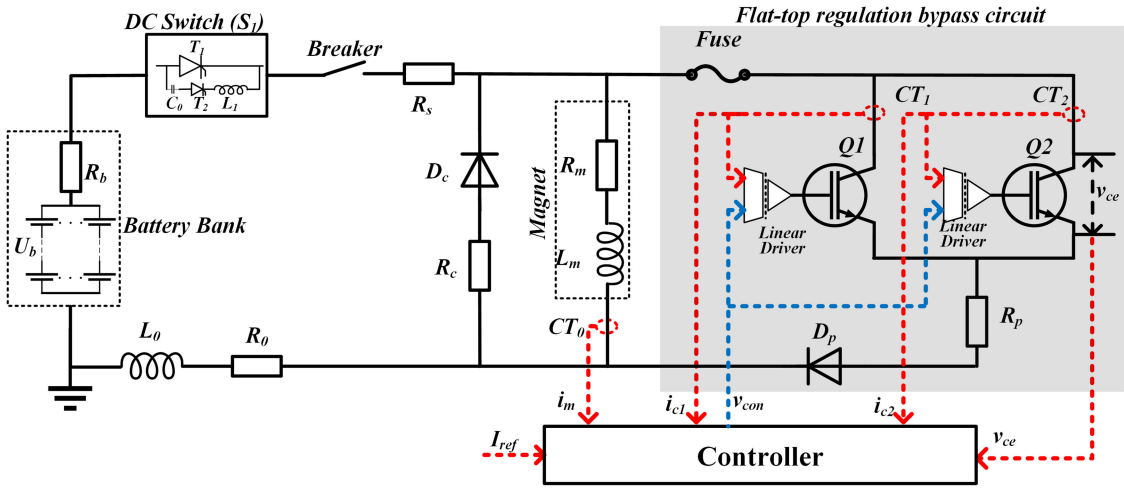

Fig. 1. FTPMF system configuration. i_m: the magnetic current; $I_{\rm ref}$: the set point of the magnetic current; i_{c1} and i_{c2}: the currents of the IGBTs; v_{ce}: the voltage of the IGBTs; $v_{\rm con}$: the control voltage of the IGBTs.

TABLE I
PERFORMANCE COMPARISON OF THE FTPMF FACILITIES

Power Supply	[Ref.]	Peak (T)	Stability (ppm)	Duration (ms)	Switch ripples (Hz)
Generator	[3]	60	…	100	660
	[4]	50	5000	100	660
Capacitor	[5]	41	2000	6.1	Free
Capacitor and Battery	[6]	60.64	82	2	Free
Battery	[7]	25	300	200	500
	This Work	23.37	65	100	free

The advantages of a stable output voltage, no ripple, and a high capacity make the battery bank a good choice for generating a relatively long FTPMF (>100 ms). However, the magnetic resistance increases slowly due to the Joule heating effect; hence, the magnetic field cannot remain constant without regulation [7]. To balance the influence of the Joule effect, a shunt-passive pulsewidth modulation (PWM) circuit was developed to obtain an FTPMF of 25 T/200 ms/300 ppm at the WHMFC [7]. Here, a 500 Hz modulation ripple is generated because the IGBTs in the bypass circuit are controlled by the PWM. Some measurement techniques that are sensitive to the ripples, such as magnetization measurement and specific heat measurement, cannot obtain high-quality data in a magnetic field with ripples [6].

In this paper, we propose a new linear flat-top regulation bypass circuit to generate a high-stability and long-duration FTPMF without switch ripples based on a battery bank power supply. In this system, the IGBT operates in the active region as a voltage-controlled current source (VCCS) to smoothly regulate the magnetic current. With this scheme, the switch ripple is eliminated, the stability of the FTPMF is greatly improved, and the duration of the flat-top is longer than 100 ms simultaneously. A performance comparison of the FTPMF facilities is listed in Table I. A 23.370 T/100 ms FTPMF with a stability of 64.2 ppm has been achieved in this paper at present, which will be used for a specific heat measurement. It is possible to generate an FTPMF with higher field strength with more IGBT modules.

The system configuration and the principle of the FTPMF system are presented in Section II. The influence of the Miller effect is analyzed, and the operating conditions of the bypass circuit are presented in Section III. Section IV analyzes the performance of the control system and presents the simulation result. Section V presents the experimental results and discussion. Finally, the conclusion and outlook are presented in Section VI.

II. SYSTEM CONFIGURATION AND WORKING PRINCIPLE

A. FTPMF System Configuration

The FTPMF system illustrated in Fig. 1 contains a pulsed magnetic field system and a flat-top regulation bypass circuit.

The pulsed magnetic field system driven by a battery bank power supply at the WHMFC has been introduced in [7] and [12]. The battery bank consists of 1400 lead-acid battery cells (12.85 V/200 Ah/3.3 mΩ internal resistance). The maximum voltage and current are 1000 V and 40 kA, respectively. R_0 and L_0 are the cable resistance and inductance, respectively. The dc switch S_1 is the main discharge switch and the breaker (Gerapid 4207) is the protection switch [7]. The crowbar branch consisting of a diode D_c and a resistor R_c is used to freewheel the magnetic current after the switch S_1 turns OFF. L_m and R_m are the magnetic resistance and inductance, respectively.

The proposed linear flat-top regulation bypass circuit consists of a fast fuse, a diode D_p, IGBTs with RC snubber circuits connected in parallel, a noninductive resistor R_p, homemade linear IGBT drivers, and a National Instruments CompactRIO 9030 controller.

The IGBTs operating in the active region are used to smoothly control the bypass current. The bypass resistor R_p can reduce

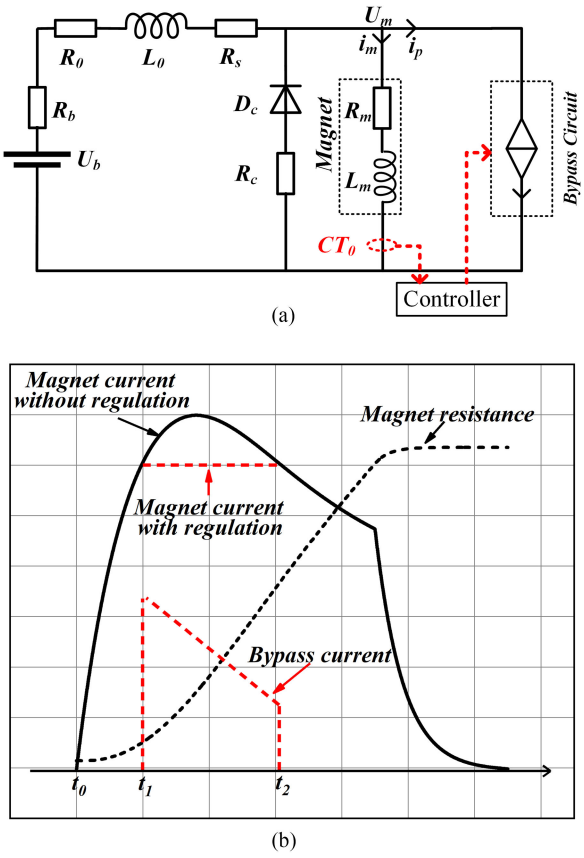

Fig. 2. (a) Equivalent circuit of the flat-top FTPMF system. (b) Sketch of the waveforms of the FTPMF system.

the power consumption of the IGBTs. The diode D_p prevents the magnetic current from freewheeling through the bypass circuit after the switch S_1 turns OFF.

B. FTPMF System Principle

The IGBT, which is equivalent to a MOSFET driving a wide base bipolar transistor in a Darlington configuration, can be in the cut-off, active or saturation region [13]. The collector current I_C is a univariant function of the gate–emitter voltage V_{GE} when an IGBT operates in the active region [13], [14], which is described as

$$I_C = \frac{1}{1-\alpha} \cdot \frac{k}{2} \cdot (V_{\mathrm{GE}} - V_{\mathrm{th}})^2 \quad (V_{\mathrm{CEth}} < V_{\mathrm{CE}} < V_{\mathrm{CES}}) \tag{1}$$

where α is the current gain of the bipolar transistor, k is the channel conductivity and depends on the geometry of the IGBT, V_{CE}, V_{th} and V_{CES} are the collector emitter voltage, the cut-in voltage, and the maximum rated voltage of the IGBT, and V_{CEth} is the threshold voltage between the active region and the saturation region.

Thus, the bypass circuit can be equivalent to a continuous VCCS when the IGBTs operate in the active region, as shown in Fig. 2(a). Theoretically, the circuit equation of the FTPMF system can be described as

$$\begin{cases} (L_m + L_0)di_m/dt + (r_m(T) + R_d)i_m \\ \qquad = U_b (t_0 \le t < t_1) \\ r_m(T)I_{\mathrm{ref}} + L_0 di_p/dt + R_d(I_{\mathrm{ref}} + i_p) \\ \qquad = U_b (t_1 \le t < t_2) \end{cases} \tag{2}$$

where $R_d = R_b + R_0 + R_s$, U_m is the magnet voltage, i_m, I_{ref}, and i_p are the magnetic current, the set point of the magnetic current, and the bypass current, respectively, t_0 is the trigger time of the switch S_1, and t_1 and t_2 are the starting and ending times of the flat-top, respectively. The magnetic resistance $r_m(T)$ is a function of the temperature of the magnet (in Kelvin) T [7], which is described as

$$\begin{cases} \dfrac{dT}{dt} = \dfrac{i_m^2 r_m(T)}{C_p(T)M} \\ C_p(T) = 834 - 4007y + 4066y^2 - 1463y^3 + 179.7y^4 \\ y = \log_{10} T \\ r_m(T) = \dfrac{-3.41 \times 10^{-9} + 7.2 \times 10^{-11} T}{-3.41 \times 10^{-9} + 7.2 \times 10^{-11} \times 77} r_m(77\,\mathrm{K}) \end{cases} \tag{3}$$

where C_p and M are the specific heat and the mass of the magnet, respectively.

Fig. 2(b) shows the relevant waveforms of the FTPMF system with and without regulation. Note that for simplicity in the exposition, the transient state of the circuit switching at time t_1 has been neglected. The working process of the FTPMF system is described as follows.

Before the moment t_1, the bypass circuit is turned OFF and the battery bank discharges to the magnet, whose current increases gradually, according to the first equation in (2).

At the moment t_1, the magnetic current i_m increases to the set point I_{ref}, and the bypass circuit starts to work. The rapid increase in the bypass current i_p results in the magnetic inductance voltage $(L_m + L_0)di_m/dt$ falling to zero, which means $i_m = I_{\mathrm{ref}}$.

During the flat-top ($t_1 < t < t_2$) period, the bypass current i_p decreases gradually with the increase in the magnetic resistance $r_m(T)$. As a result, the magnetic current can remain a constant value of I_{ref}. Then, S_1 switches OFF, and the magnet current freewheels through the crowbar branch.

When the IGBTs operate in the active region, the switching ripples caused by the PWM are avoided, and the stability of the FTPMF can be improved.

III. Design of the Bypass Circuit

According to the system principle, the IGBTs must always operate in the active region during the flat-top period. Hence, the collector emitter voltage V_{CE} should be higher than the threshold voltage V_{CEth}

$$V_{\mathrm{CE}} = I_{\mathrm{ref}} r_m(T) - i_p R_p > V_{\mathrm{CEth}}. \tag{4}$$

Another consideration is the influence of the Miller effect, which is caused by the capacitance between the gate and the

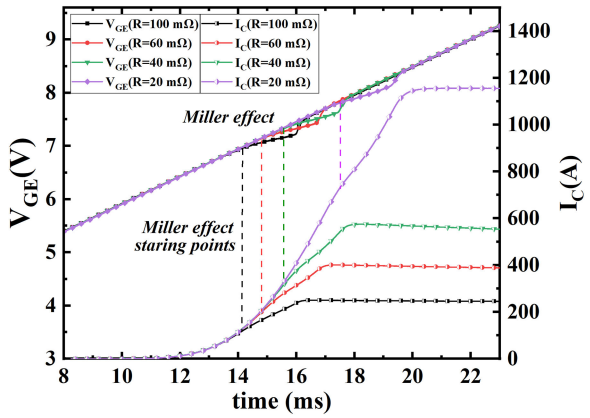

Fig. 3. Experimental results of the Miller effect test.

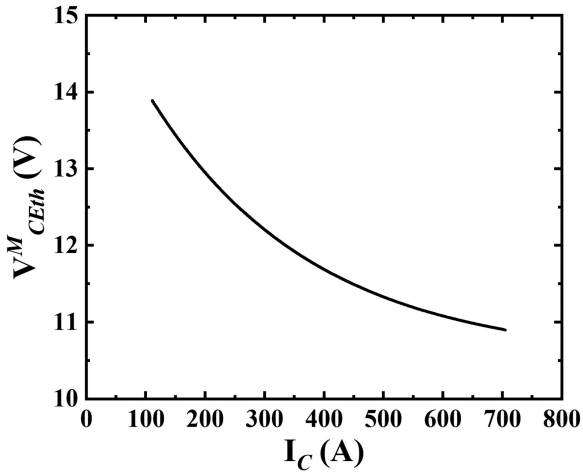

Fig. 4. Experimental results of the threshold voltage of the Miller effect.

collector C_{GC}, called the Miller capacitance. The Miller capacitance can be approximated as a two-step function of the collector–emitter voltage [17]–[19]

$$C_{\mathrm{GC}(V_{\mathrm{CE}})} = \begin{cases} C_{\mathrm{GC1}}, & V_{\mathrm{CE}} \le V^{M}_{\mathrm{CEth}} \\ C_{\mathrm{GC2}}, & V_{\mathrm{CE}} > V^{M}_{\mathrm{CEth}} \end{cases} \tag{5}$$

where V^{M}_{CEth} is the threshold voltage of the Miller effect.

The variation in the capacitance C_{GC} will cause an out-of-control gate voltage V_{GE}: The gate voltage V_{GE} is lower or higher than the control voltage when the capacitance C_{GC} increases or decreases, respectively. This is the reason for generating the "Miller platform" and the "tail current" during the IGBT turn-ON and turn-OFF in switched-mode operation [13], [15]–[18].

The control voltage is continuous rather than the pulsed when the IGBT operates in the active region, which makes the "source current" and "sink current" of the driver small. When the capacitance C_{GC} suddenly changes, the driver cannot absorb or replenish the charge quickly due to the limitation of the drive current. Therefore, the Miller effect will last longer. In the FTPMF system, the Miller effect can cause the magnetic current to oscillate, so it is necessary to avoid it.

The Miller effect of the FZ3600R17KE3-B2 used in our system is tested. In the test, the power supply voltage is 25 V, and a variable resistor *R* is used in series with an IGBT. The gate resistance R_{G-EX} and capacitance $C_{\mathrm{GE}-EX}$ of the IGBT are set to 10 Ω and 2.7 μF, respectively. The variable resistor *R* is taken to be 20, 40, 60, and 100 mΩ. Loading a ramp voltage to the control voltage, the current I_C increases with the increase in the control voltage, and the voltage V_{CE} decreases gradually until the IGBT is fully turned ON.

Fig. 3 shows the experimental results of the Miller effect. The experimental result suggests that the threshold voltage of the Miller effect V^{M}_{CEth} is related to the collector current I_C instead of a constant. The Miller effect can be neglected when the voltage V_{CE} is higher than the threshold voltage $V^{M}_{\mathrm{CEth}}(I_C)$; otherwise, the gate voltage cannot follow the control voltage until the IGBT is fully turned ON. According to the I_C–V_{GE} curve, the function of $I_C = f(V_{\mathrm{GE}})$ still conforms to the transfer characteristic during the Miller effect, which suggests $V^{M}_{\mathrm{CEth}}(I_C) > V_{\mathrm{CEth}}$. The test result of $V^{M}_{\mathrm{CEth}}(I_C)$ is shown in Fig. 4. Accordingly, the bypass resistor R_p and the set point of the magnetic current I_{ref} should meet the following requirement:

$$\begin{cases} V_{\mathrm{CE}} = I_{\mathrm{ref}} r_m(T) - i_p R_p > V^{M}_{\mathrm{CEth}}(I_C) \\ i_p = N \cdot I_C \end{cases} \tag{6}$$

where *N* is the number of IGBTs connected in parallel.

The power consumption of an IGBT is large when it operates in the active region [19], [20]. The IGBT module cannot reach thermal balance in a short time, so most of the heat is absorbed by its heat capacity in the pulse power system. In this case, it is critical to monitor the junction temperature to protect the IGBT. However, it is impossible to use a temperature sensor to measure the junction temperature of the IGBT in an unsteady system. Consequently, we use the instantaneous thermal model of the IGBT module, the Foster model [20], to calculate the real-time junction temperature. The bypass circuit will turn OFF when the junction temperature of the IGBTs exceeds the protective threshold.

IV. Control System Design and Simulation

The FTPMF system is a nonlinear time-varying system because the magnetic resistance R_m varies with time due to the Joule heating.We regard the system as a dynamic regulation system under a quiescent operation point driven by the battery bank power supply. The quiescent operation point can be calculated by

$$I_{pq} = \left(U_b - (\bar{R}_m + R_d) I_{\mathrm{ref}}\right) / R_d \tag{7}$$

where $\bar{R}_m$ is the average of the magnetic resistance and I_{pq} is the quiescent operation point of the bypass current.

The dynamic control system is a dual closed-loop system. The inner feedback loop is used to optimize the nonlinearity and high sensitivity of the transfer characteristic of the IGBT [21], and it can effectively suppress the thermal effect of the IGBT, which is a negative temperature characteristic, to avoid the risk of a

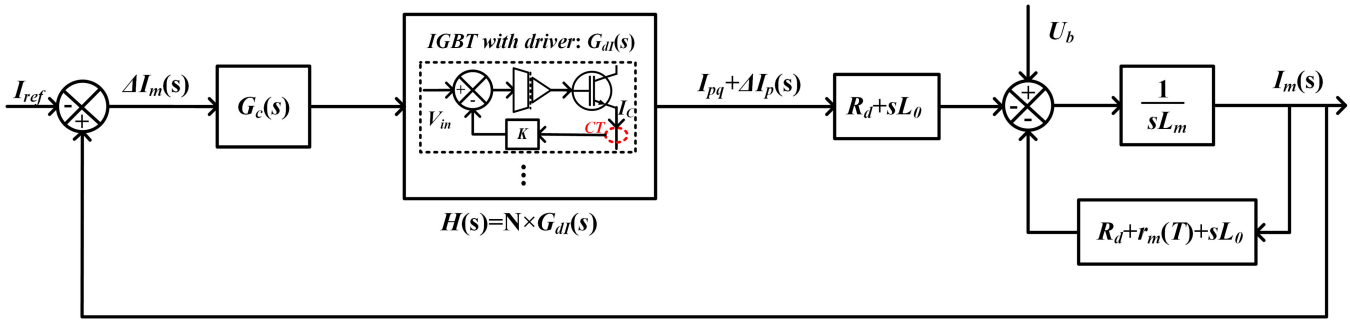

Fig. 5. Diagram of the closed-loop control system.

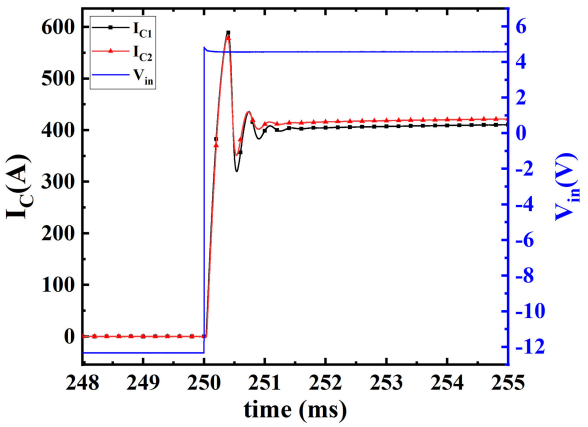

Fig. 6. Step response of the IGBT (FZ3600R17KE3-B2) with the driver.

thermal runaway of the IGBTs in parallel [21], [22]. The outer feedback loop is used to stabilize the magnetic current.

Fig. 5 shows a diagram of the closed-loop control system. Δ represents the dynamic variation in the corresponding physical quantity. The open-loop transfer function of the dynamic control system is

$$G_k(s) = \frac{G_c(s)H(s)(R_d + L_0 s)}{(R_d + r_m(T)) + (L_m + L_0)s} \tag{8}$$

where $G_c(s)$ is the transfer function of the proportional–integral (PI) controller, $H(s) = N \times G_{dI}(s)$ is the transfer function of the IGBTs with drivers in parallel, and the parallel branch number N is 2 in the prototype.

The step response from the driver to the IGBT is shown in Fig. 6. The vertical axes are the collector current of the IGBT I_C and driving voltage V_{in}, respectively. The dynamic performances of the two IGBTs with drivers are almost identical, and the transmission delay, rise time, and stabilization time are 10 μs, 180 μs, and 790 μs, respectively. Their steady-state gains are 91.73 and 88.57, respectively. The transfer function of the IGBT with the driver, $G_{dI}(s)$, can be approximated as

$$G_{dI}(s) = \frac{I_C(s)}{V_{\text{in}}(s)} = \frac{90e^{-10^{-5}s}}{(1.03 \times 10^{-4}s)^2 + 8.24 \times 10^{-5}s + 1}. \tag{9}$$

TABLE II
SPECIFICATIONS OF THE SYSTEM PARAMETERS

Circuit parameters	Cable resistance R_0	8 mΩ
	Cable inductance L_0	40 μH
	Series resistor R_s	15 mΩ
	Bypass resistor R_p	146 mΩ
	Crowbar resistor R_c	10 mΩ
	Bypass IGBTs	FZ3600R17KE3-B2
	Diodes	DZ3600S17K3
Battery bank	Battery number	720
	Parallel branch number	12
	Number per branch	60
	Output voltage U_b	771 V
	Internal resistance R_b	16.5 mΩ
Magnet	Inductance L_m	8 mH
	Resistance R_m	6.2 mΩ (77K)
	Coil constant	1.4T/kA
	Ambient temprature	15 °C

The circuit parameters of the prototype system are listed in Table II. To simplify the analysis, we consider an even number of values within the range of variation in the magnetic resistance $r_m(T)$ to analyze the stability of the system. Fig. 7 shows a Bode diagram with different P parameters of the PI controller and the magnetic resistance varying from 6 to 24 mΩ (with an interval of 3 mΩ) for every colored curve. The analysis indicates that the magnetic resistance does not influence the performance of the system when the frequency is higher than 20 Hz. The crossover frequency of the system will be lower than 30 Hz when the P parameter is lower than 0.08, which leads to a poor dynamic performance. The phase margin will be lower than 30° when the P parameter is higher than 0.25 and the system is not stable enough [23]. According to the pole-zero analysis, the system order will be reduced when the integral time constant T_i is equal to the loop time constant, which means the system performance is optimal.

With $P = 0.2$, a phase margin of 35°, and a crossover frequency of 3 kHz, a 16.7 kA (23.37 T)/100 ms/12 ppm flat-top profile is achieved by the state-space model. The simulation is based on an ideal environment that ignores the sampling error and measurement noise.

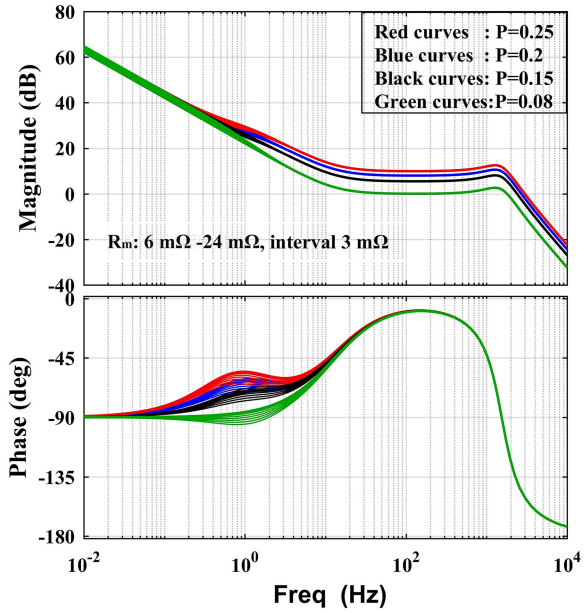

Fig. 7. Bode diagram of the dynamic system with different *P* parameters and the magnetic resistance varying from 6 to 24 mΩ for every colored curve.

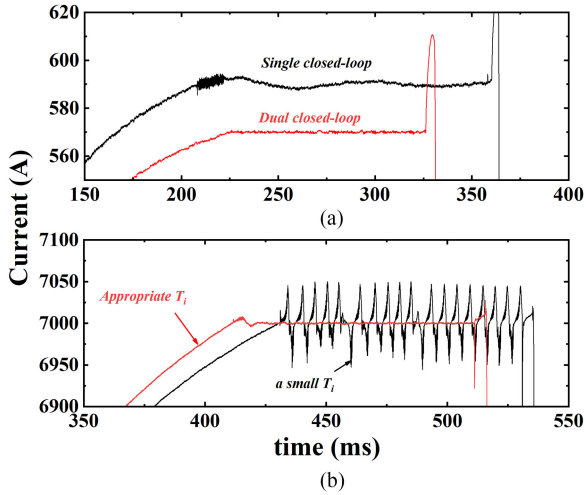

Fig. 8. Experimental results of the system pretest. (a) Comparison of the single and dual closed-loop control. (b) Influence of the integral time.

V. Experimental Results and Discussion

The test circuit is shown in Fig. 1, and the main experimental parameters are listed in Table II. The cable resistance R_0 and inductance L_0, series resistor R_s, bypass resistor R_p, and crowbar resistor R_c are 8 mΩ, 40 μH, 15 mΩ, 146 mΩ, and 10 mΩ, respectively. The two IGBTs of FZ3600R17KE3-B2 and a diode of DZ3600S17K3 are used in the bypass circuit. The voltage of the battery bank (12 parallel branches and 60 cells per branch) is set at 771 V with an internal resistance of 16.5 mΩ. The magnetic resistance R_m and inductance L_m are 6.2 mΩ (77 K) and 8 mH, respectively, and the coil constant of the magnet is 1.4 T/kA.

The protective thresholds of the current (3000 A) and the junction temperature (120 °C) of the IGBTs are set. A 16-bit analog-to-digital converter (ADC) is utilized to acquire the signals of the sensors. The sample frequency of the ADC is 100 kHz and the control period of the PI controller is 0.2 ms. The magnetic current is measured by a high-stability Hall current sensor [7]. The magnetic field is measured by a pick-up coil calibrated by the quantum oscillation effect.

A. Experiment on the Control System Performance

Some experimental results of the system pretest are illustrated in Fig. 8.

Fig. 8(a) depicts an experimental comparison of the single and dual closed-loop control systems. The set points of the magnetic current are 590 and 570 A, respectively. It is almost impossible to achieve a high-precision adjustment of the magnetic current with single closed-loop control due to the nonlinearity of the transfer characteristic of the IGBT. The system has good performance with dual closed-loop control, and the parameters of the controller are easy to select according to the analysis above. The experimental result is very good when the *P* parameter is between 0.18 and 0.22.

Fig. 8(b) shows the influence of the integral time T_i. If T_i is less than 1/2 of the loop time constant, the magnetic current will oscillate. The jump of the magnetic current after the flat-top period is caused by the forced commutation of the switch S_1 [12].

B. Experiment on the FTPMF

A 16.7 kA (23.37 T)/100 ms flat-top profile is accomplished by the experiment at the WHMFC, as shown in Fig. 9.

Fig. 9(a) shows the battery bank current I_s, magnetic current I_m, and the current I_C and voltage $V_{\rm CE}$ of the IGBTs. The waveforms of the current of the bypass circuit $I_p = I_{C1} + I_{C2}$ and magnet I_m are consistent with the discussion in Section II-B. The battery bank current is $I_s = I_m + I_p$. Fig. 9(b) presents the temperature rise of junction (ΔT*vj*) and the power of the IGBTs.

The stabilization time of the control system is approximately 8 ms, and there is an oscillation of the magnetic current of $\pm$ 5 A/5 kHz during the transition, which is explained as follows.

During the flat-top period (from 510 to 610 ms), the magnetic current is 16.7 kA $\pm$ 1 A; the currents of the IGBT1 I_{C1} and IGBT2 I_{C2} are approximately from 425 to 105 A and from 435 to 130 A, respectively. The current sharing coefficient *K*, which is defined as the ratio of the average to the maximum [see (10)], is from 0.99 to 0.9, which is a good result. The voltage of the IGBTs ranges from 23 to 125 V. The maximum powers and the increase in the junction temperatures of the IGBTs are 19.8 kW, 21 kW, and 82 °C, 90 °C, respectively, which suggest that the IGBTs are secure. The differences of the two IGBTs increase gradually due to the negative temperature characteristic of the transfer characteristic. The magnetic resistances before and after discharge are 6.2 and 12 mΩ, respectively.

$$K = \frac{\text{Aver}(I_{C1}, I_{C2})}{\text{Max}(I_{C1}, I_{C2})}. \tag{10}$$

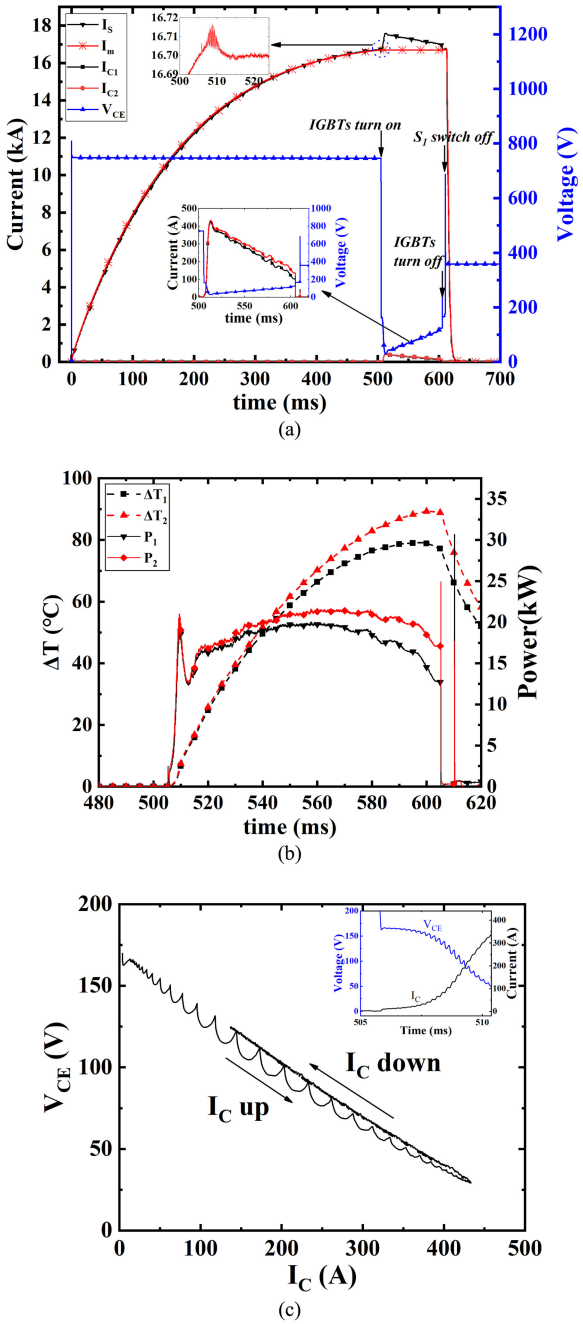

Fig. 9. Experimental results. (a) Battery-bank current I_s, magnetic current I_m,[a] and the current I_C and voltage $V_{\rm CE}$[b] of IGBTs. (b) Junction temperature rise and power of the IGBTs. (c) Curve of $V_{\rm CE}(I_C)$ during the flat-top.[a] The freewheeling current is not measured as the crowbar branch is connected to the magnet electrode directly; therefore, the current of the battery-bank and magnet drop rapidly. [b] Because of the presence of the diodes D_p and the *RC* snubber circuits, the voltage $V_{\rm CE}$ cannot reduce when the IGBTs turn OFF.

Fig. 9(c) shows a curve of $V_{\rm CE}(I_C)$ during the flat-top period, and it indicates that the $V_{\rm CE}(I_C)$ is higher than the threshold voltage of the Miller effect $V^M_{\rm CEth}(I_C)$ (see Fig. 4); therefore, the Miller effect will not occur. However, there is a slight oscillation of the magnetic current before the system becomes stable [see the inset and I_C in Fig. 9(c)]. Although the variation in the Miller capacitance is small when $V_{\rm CE}(I_C) > V^M_{\rm CEth}(I_C)$, the rapid

TABLE III
COMPARISON OF THE EXPERIMENTAL AND SIMULATION RESULTS DURING THE FLAT-TOP PERIOD

	Simulation	Experiment
Magnet current I_m	16.7 kA	16.7 kA
Stabilization time	5 ms	8 ms
Stability of the FTPMF	12 ppm	65 ppm
Magnet resistance	6.2 mΩ - 11.7 mΩ	6.2 mΩ - 12 mΩ
IGBT current I_C	450 A - 100 A	430 A - 117 A
IGBT voltage V_{CE}	25 V - 140 V	23 V - 125 V
IGBT maximum Power	23 kW	20 kW
IGBT maximum ΔT_{vj}	93 °C	86 °C

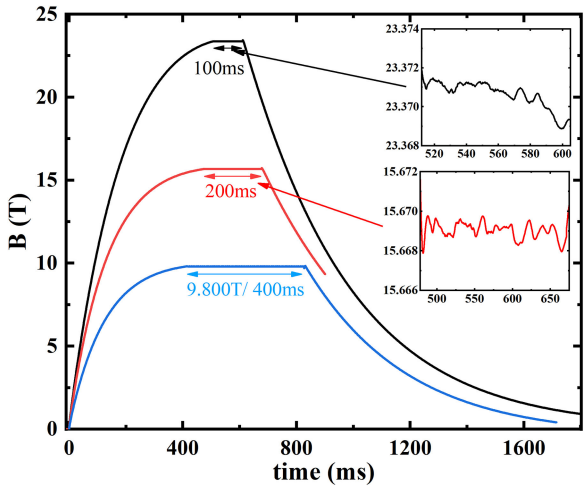

Fig. 10. Experimental results of the magnetic field.

changes in the voltage $V_{\rm CE}$ can also cause enough charge transfer to cause a slight Miller effect, which causes the oscillation of the magnetic current I_m [see Fig. 9(a)]. After the system becomes stable, the change in the voltage $V_{\rm CE}$ is slow and the variation in the Miller capacitance is small so that the Miller effect is avoided.

A comparison of the experimental and simulation results during the flat-top period is given in Table III, where the experimental results of the IGBT are average values. The experimental and simulation results are in good agreement except for the stability, which is much better in the simulation (12 ppm) than in the experiment (65 ppm). The difference in the stability is mainly caused by the measurement system. The sampling resolution of the magnetic current is 0.3 A (18 ppm) in the prototype so that the stability cannot be better than 18 ppm, and the measurement noise, which is difficult to quantify, can also affect the stability in the experiment. It is possible to improve the stability by using 24-bit ADC and a direct-current current transformer [24], which is very expensive.

In addition, experiments on the 11.2 kA/200 ms and 7 kA/400 ms FTPMFs are also completed with battery bank voltages of 694 and 465 V. Fig. 10 presents the corresponding experimental results of the magnetic field. The performance parameters of the FTPMFs are 23.370 T/100 ms/64.2 ppm (black),

15.699 T/200 ms/63.8 ppm (red), and 9.800 T/400 ms/70 ppm (blue). As expected, there are no high-frequency switch ripples during the flat-top period, the stability of the FTPMF is improved greatly, and the duration is longer than 100 ms simultaneously.

VI. Conclusion

In this paper, a high-stability FTPMF system with a new linear regulation bypass circuit is presented. In the system, the IGBTs operate in the active region to smoothly regulate the current to avoid switch ripples and improve the stability of the FTPMF. An accurate model of the FTPMF system is developed, which can be used to guide the construction of an FTPMF system. With this scheme, the stability of the FTPMF has been improved to 65 ppm to meet the requirement of high-precision scientific experiments. The FTPMF of 23.37 T/100 ms/64.2 ppm will be used for a specific heat measurement and the FTPMF of 40 T/$\pm$0.0015 T is under construction at the WHMFC.

References

[1] F. Herlach, "Pulsed magnets," *Rep. Prog. Phys.*, vol. 62, no. 6, pp. 859–920, Jun. 1999.

[2] F. Weickert *et al.*, "Implementation of specific-heat and NMR experiments in the 1500 ms long-pulse magnet at the Hochfeld-Magnetlabor Dresden," *Meas. Sci. Technol.*, vol. 23, no. 10, Jul. 2012, Art. no. 105001.

[3] L. Campbell, H. Boenig, D. Rickel, J. Schillig, H. Schneider-Muntau, and J. Sims, "The NHMFL long-pulse magnet system—60–100 T," *Phys. B, Condens. Matter*, vol. 216, no. 3/4, pp. 218–220, 1996.

[4] H. Ding *et al.*, "Design of a 135 MW power supply for a 50 T pulsed magnet," *IEEE Trans. Appl. Supercond.*, vol. 22, no. 3, Jun. 2012, Art. no. 5400504.

[5] F. Jiang *et al.*, "Design and test of a flat-top magnetic field system driven by capacitor banks," *Rev. Sci. Instrum.*, vol. 85, no. 4, Apr. 2014, Art. no. 045106,

[6] Y. Kohama and K. Kindo, "Generation of flat-top pulsed magnetic fields with feedback control approach," *Rev. Sci. Instrum.*, vol. 86, no. 10, Oct. 2015, Art. no. 104701

[7] H. Xiao *et al.*, "Development of a high-stability flat-top pulsed magnetic field facility," *IEEE Trans. Power Electron.*, vol. 29, no. 9, pp. 4532–4537, Sep. 2014.

[8] X. T. Han *et al.*, "The pulsed high magnetic field facility and scientific research at Wuhan National High Magnetic Field Center," *Matter Radiat. Extremes*, vol. 2, no. 6, pp. 278–286, Nov. 2017.

[9] J. Cravero and J. Royer, "The IGBT as an element of switch discharge with a linear mode use in capacitor discharge power converters," CERN-PS-98-053-PO, 1998.

[10] D. Aguglia, "Design of a system of high voltage pulsed power converters for CERN's Linac4 H^- ion source," in *Proc. 19th IEEE Pulsed Power Conf.*, 2013, pp. 1–6.

[11] J.-M. Cravero, F. C. Magallanes, R. G. Retegui, S. Maestri, and G. Uicich, "Control of high power IGBT modules in the active region for fast pulsed power converters," in *Proc. 15th Eur. Conf. Power Electron. Appl.*, 2013, pp. 1–8.

[12] T. Ding *et al.*, "The design and tests of battery power supply system for pulsed flat-top magnets in WHMFC," *J. Low Temp. Phys.*, vol. 170, no. 5/6, pp. 481–487, Nov. 2013.

[13] A. Sattar, "Insulated gate bipolar transistor (IGBT) basics," 2010. [Online]. Available: http://www.ixys.com/Documents/AppNotes/IXYS_IGBTBasic I.pdf

[14] J. Lutz, H. Schlangenotto, U. Scheuermann, and R. De Doncker, *Semiconductor Power Devices: Physics, Characteristics, Reliability*. New York, NY, USA: Springer, 2011, pp. 391–422.

[15] P. J. Grbovic, "An IGBT gate driver for feed-forward control of turn-on losses and reverse recovery current," *IEEE Trans. Power Electron.*, vol. 23, no. 2, pp. 643–652, Mar. 2008.

[16] I. Baraia, J. A. Barrena, G. Abad, J. M. C. Segade, and U. Iraola, "An experimentally verified active gate control method for the series connection of IGBT/diodes," *IEEE Trans. Power Electron.*, vol. 27, no. 2, pp. 1025–1038, Feb. 2012.

[17] M. Cotorogea, "Physics-based SPICE-model for IGBTs with transparent emitter," *IEEE Trans. Power Electron.*, vol. 24, no. 12, pp. 2821–2832, Dec. 2009.

[18] P. R. Palmer, E. Santi, J. L. Hudgins, X. S. Kang, J. C. Joyce, and P. Y. Eng, "Circuit simulator models for the diode and IGBT with full temperature dependent features," *IEEE Trans. Power Electron.*, vol. 18, no. 5, pp. 1220–1229, Sep. 2003.

[19] U.-M. Choi, F. Blaabjerg, and S. Jørgensen, "Study on effect of junction temperature swing duration on lifetime of transfer molded power IGBT modules," *IEEE Trans. Power Electron.*, vol. 32, no. 8, pp. 6434–6443, Aug. 2017.

[20] A. Volke, J. Wendt, and M. Hornkamp, *IGBT Modules:Technologies, Driver and Application*. Neubiberg, Germany: Infineon, 2012, pp. 118–138.

[21] D. Bortis, J. Biela, and J. W. Kolar, "Active gate control for current balancing of parallel-connected IGBT modules in solid-state modulators," *IEEE Trans. Plasma Sci.*, vol. 36, no. 5, pp. 2632–2637, Oct. 2008.

[22] H. A. Mantooth, K. Peng, E. Santi, and J. L. Hudgins, "Modeling of wide bandgap power semiconductor devices-part I," *IEEE Trans. Electron Devices*, vol. 62, no. 2, pp. 423–433, Feb. 2015.

[23] A. Isidori, *Nonlinear Control Systems*. New York, NY, USA: Springer, 2013, pp. 145–226.

[24] M. C. Bastos *et al.*, "High accuracy current measurement in the main power converters of the large hadron collider: Tutorial 53," *IEEE Instrum. Meas. Mag.*, vol. 17, no. 1, pp. 66–73, Feb. 2014.

Shaozhe Zhang received the B.S. degree in electrical and electronics engineering from the Shenyang University of Technology, Shenyang, China, in 2014. He is currently working toward the Ph.D. degree with the Huazhong University of Science and Technology, Wuhan, China.

His principle research interests include pulse power technology, power electronics, and high-current measurement.

Zhenglei Wang received the B.S. degree in electrical and electronics engineering in 2018 from the Huazhong University of Science and Technology, Wuhan, China, where he is currently working toward the M.S. degree.

His principle research interests include pulse power technology and power electronics.

Tonghai Ding received the B.S. degree from the Huazhong University of Science and Technology, Wuhan, China, in 1994, and the Ph.D. degree from the Chinese Academy of Sciences, Hefei, China, in 2007.

From July 1994 to November/December 2007, he was with the Chinese Academy of Sciences as an Engineer. Since December 2007, he has been working with Wuhan National High Magnetic Field Center. He is currently a Professor with the Huazhong University of Science and Technology, China. His principle research interests include pulse power technology and power electronics.

Houxiu Xiao received the B.S. and Ph.D. degrees in electrical and electronics engineering from the Huazhong University of Science and Technology, Wuhan, China, in 2004 and 2009, respectively.

From 2010 to 2011, he was a Postdoctoral Researcher with the Laboratoire National des Champs Magn´etiques Intenses, CNRS, Grenoble, France. Since 2011, he has been working with Wuhan National High Magnetic Field Center. He is currently an Associate Professor with the Huazhong University of Science and Technology. His principle research interests include the generation and application of pulsed magnetic fields, pulse power technology, high-stability large current sources, pulsed magnet technology, and pulsed power supplies.

Jianfeng Xie received the B.S. degree from the Changsha University of Science and Technology, Changsha, China, in 1998, and M.S. degree from the Huazhong University of Science and Technology, Wuhan, China, in 2005, respectively.

Since March 2008, he has been working with Wuhan National High Magnetic Field Center. He is a Senior Engineer with the Huazhong University of Science and Technology. His principle research interests include electromagnetic measurements and power electronics.

Xiaotao Han (M'17) received the B.S. and the Ph.D. degrees in electrical and electronics engineering from the Huazhong University of Science and Technology, Wuhan, China, in 1996 and 2004, respectively.

From July 2005 to October 2011, he was with the College of electrical and electronic engineering, Huazhong University of Science and Technology. Since November 2011, he has been working with Wuhan National High Magnetic Field Center. He is a Professor with the Huazhong University of Science and Technology. His principle research interests include electromagnetic measurements, signal processing, and application technology of the high magnetic field.